Coherent metallic screening in core-level photoelectron spectra for the strongly correlated oxides $La_{1-x}Ba_xMnO_3$ and $V_{1-x}W_xO_2$

S. Ueda,[1,2] H. Takami,[2] T. Kanki,[2] and H. Tanaka[2]

[1]*Synchrotron X-ray Station at SPring-8, National Institute for Materials Science (NIMS), Sayo, Hyogo 679-5148, Japan*

[2]*The Institute of Scientific and Industrial Research, Osaka University, Ibaraki, Osaka 567-0047, Japan*

(Received 16 May 2013; published 28 January 2014)

Coherent metallic screening structures shown in core-level photoemission spectra for strongly correlated oxide materials were studied by hard x-ray photoemission spectroscopy (HAXPES) and the configuration interaction (CI) theory based on the cluster model, including the coherent metallic screening process. For the $La_{1-x}Ba_xMnO_3$ thin film, the normalized intensity of the coherent metallic screening structure (I_S) seen in the Mn $2p$ core-level spectra was proportional to the square of the hybridization strength, $(V^*)^2$, between the transition metal $3d$ and coherent metallic states. In contrast, the normalized I_S seen in the V $2p$ core-level spectra for the $V_{1-x}W_xO_2$ thin film was not proportional to $(V^*)^2$. The different behaviors of the normalized I_S for the $La_{1-x}Ba_xMnO_3$ and $V_{1-x}W_xO_2$ thin films as a function of V^* were understood by the series of the CI cluster model calculation. From the CI cluster model calculation, we found that the charge transfer energy (Δ^*) between the transition metal $3d$ states and the coherent metallic states strongly affect the normalized I_S in the $2p$ core-level photoemission final states. Therefore, the behavior of the normalized I_S in the $2p$ core-level HAXPES is thus not simply explained by the change of V^*. The electronic structure parameters such as Δ^* and V^* relating to the coherent metallic states strongly contribute to the variation of the normalized I_S in the photoemission final states. In contrast, we found that the detailed I_S evaluation in the core-level HAXPES experiments for materials, in which the coherent metallic screening structures appear, allows us to evaluate the value of V^* when we have the experimental core-level spectra and the electronic structure parameters set for a reference material. We also found that the intensity at the Fermi level is proportional to $(V^*)^2$, as expected from the Anderson impurity model.

DOI: 10.1103/PhysRevB.89.035141 PACS number(s): 79.60.Dp, 71.27.+a, 31.15.−p

I. INTRODUCTION

Strongly correlated oxides exhibit a satellite structure in core-level photoemission due to a coherent metallic screening (in other words, nonlocal screening) effect [1–3]. In particular, hard x-ray photoemission spectroscopy (HAXPES) revealed this kind of satellite structure in perovskite-type Cu and Mn oxides [3–7] and V oxides [8–12] because of a large probing depth in HAXPES measurements [13–15]. For $La_{1-x}Ba_xMnO_3$ thin films, the intensity of the satellite structure (I_S) strongly depends on temperature in the ferromagnetic metal phase [6,7]. In addition, the presence of the satellite in the Mn $2p$ core-level HAXPES spectra for $La_{1-x}Sr_xMnO_3$ thin films indicates the finite density of states (DOS) at the Fermi level (E_F) [4,16]. For $V_{1-x}W_xO_2$ thin films in the metallic phase, the V $2p$ core-level HAXPES spectra also show the satellite structure due to the coherent metallic screening effect and show that I_S depends on the W-doping concentration, as mentioned later. This coherent metallic screening process arises from the hybridization (V^*) between the transition metal $3d$ states and coherent metallic band at around E_F. According to the Anderson impurity model (AIM) [16], DOS at E_F is proportional to $(V^*)^2$. To understand the electronic structure of the strongly correlated system, which shows the coherent metallic screening effect in the core-level spectra, it is important to clarify the relationship between I_S, V^*, and DOS at E_F from both the experimental and theoretical approaches. In this paper, we investigate the electronic structures of $La_{1-x}Ba_xMnO_3$ and $V_{1-x}W_xO_2$ thin films by means of HAXPES and the configuration interaction (CI) theory based on the cluster model, including the coherent metallic screening process. For $La_{1-x}Ba_xMnO_3$ thin films, the magnetization and conductivity of the films were well reproduced by Bloch $T^{3/2}$ law using temperature-dependent ferromagnetic interaction (J), which is proportional to $(V^*)^2$ [7]. The linear relationship between I_S and $(V^*)^2$ has been shown by the previous experiment [6]. This linear relationship, however, has not been clarified by the theoretical calculation. In addition, the relationship between DOS at E_F and V^* has not been clarified by the experiments. Here we also investigate the relationship between DOS at E_F and V^* by the combination of the HAXPES experiments and the CI cluster model calculation, which includes the coherent metallic screening process.

II. EXPERIMENT

A 20-nm-thick $La_{1-x}Ba_xMnO_3$ thin film with $x = 0.15$ was grown on an etched Nb-doped $SrTiO_3$ substrate by a pulsed laser deposition (PLD) method. The details of the sample growth and physical properties were described in Ref. [6]. $V_{1-x}W_xO_2$ thin films with a thickness of 110–186 nm and $x = 0.0 - 0.05$ were also grown on $Al_2O_3(0001)$ substrates by a PLD method. The detail sample preparation and physical properties were described elsewhere [17,18]. The HAXPES measurements for the $La_{1-x}Ba_xMnO_3$ thin film were performed at the undulator beamline BL29XU of SPring-8. The sample was cooled by a He flow-type refrigerator. The HAXPES measurements for the $V_{1-x}W_xO_2$ thin films were performed at the undulator beamline BL15XU [19] of SPring-8. The sample temperature was set to 360 K. At this temperature, all of the $V_{1-x}W_xO_2$ thin films are in the metallic phase [17,18]. Total energy resolution of the HAXPES measurements was set to about 240 meV. Base pressure of an

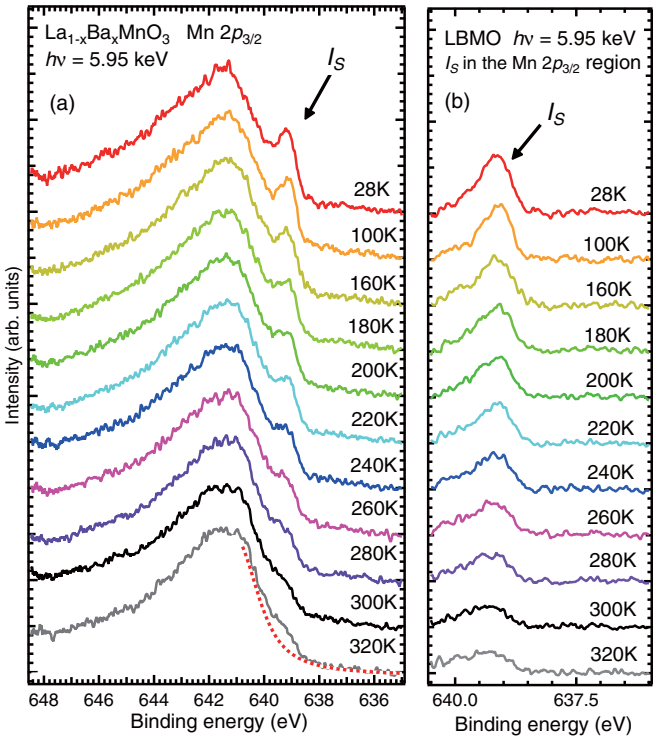

FIG. 1. (Color online) (a) Mn $2p$ core-level HAXPES spectra of the $La_{1-x}Ba_xMnO_3$ thin film with $x = 0.15$ taken at various temperature [6]. (b) I_S spectra obtained by subtracting the assumed tail spectrum from the Mn $2p$ core-level HAXPES spectra.

analysis chamber attached to a high-resolution hemispherical electron analyzer (VG Scienta R4000) was better than 1×10^{-7} Pa.

III. RESULTS

Figure 1 shows the temperature-dependent Mn $2p$ core-level spectra for the 20-nm-thick $La_{1-x}Ba_xMnO_3$ thin film with $x = 0.15$ [6]. While decreasing the sample temperature, I_S in the Mn $2p$ core-level spectra located at the binding energy (E_B) of 639.3 eV increased. At various temperatures, the values of V^* were estimated from the CI cluster model calculation in Ref. [6]. Figure 2(a) shows I_S as a function of $(V^*)^2$, reported in Ref. [6]. A clear linear relationship between I_S and $(V^*)^2$ was found. In Fig. 2(a), I_S was measured against the spectrum taken at 320 K; therefore, I_S does not go through the origin of the figure. Assuming the baseline shape (dashed line; Fig. 1), we evaluated the normalized I_S relative to the Mn $2p_{3/2}$ photoemission intensity, which excludes I_S as a function of $(V^*)^2$ in Fig. 2(b). The linear relationship between the normalized I_S and $(V^*)^2$ with the zero-crossing behavior in Fig. 2(b) was obvious.

Figure 3 shows the temperature-dependent valence-band HAXPES spectra of the $La_{1-x}Ba_xMnO_3$ thin film in the vicinity of E_F. The valence-band spectra for the $La_{1-x}Ba_xMnO_3$ thin film were normalized by the integrated intensity of the whole valence-band region. The peak and hump structures around 2 eV and E_F were assigned to the Mn $3d$ t_{2g} and e_g states, respectively. The intensity at E_F ($I(E_F)$) increased with the decreasing of the sample temperature. In addition,

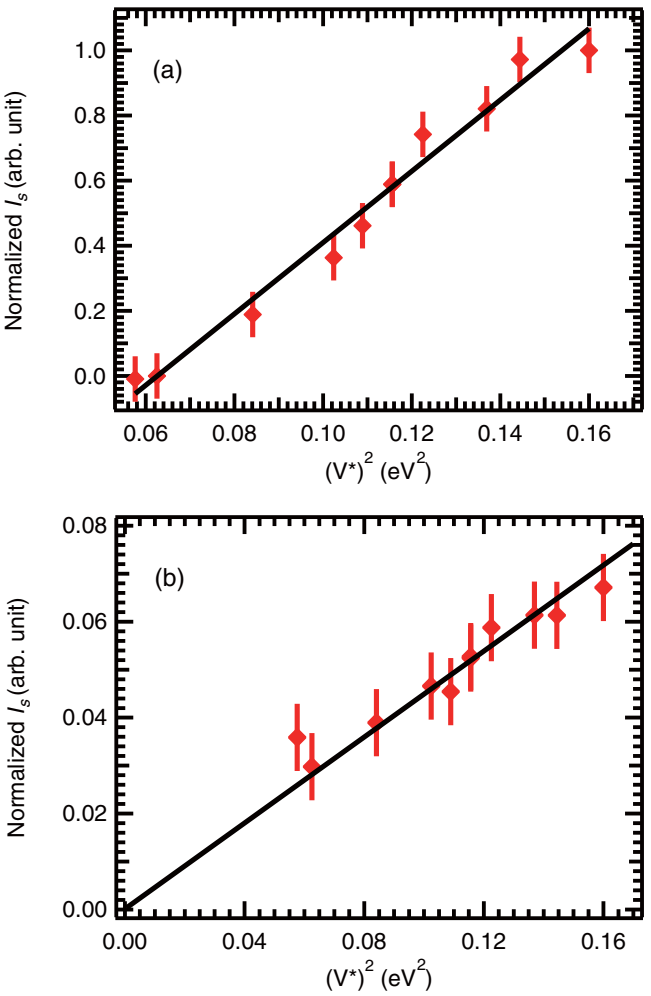

FIG. 2. (Color online) (a) I_S referred to the spectrum taken at 320 K as a function of $(V^*)^2$, where I_S was normalized by the Mn $2p$ main peak intensity. (b) I_S obtained by subtracting the assumed tail spectrum from the Mn $2p$ core-level spectra as a function of $(V^*)^2$, where I_S was normalized by $(I_{Mn2p} - I_S)$. The values of V^* were obtained from Ref. [6].

the t_{2g} states around 2 eV shifted to the higher E_B side with the increasing of the sample temperature. The energy shift of the t_{2g} states was understood by the destabilization of the ferromagnetic states [5].

Figure 4 shows the V $2p$ core-level spectra for the $V_{1-x}W_xO_2$ thin films taken at 360 K. As seen in Fig. 4, I_S increases with the increasing of the W concentration. For the V $2p$ core-level spectra, the satellite structure does not show a sharp peak structure, in contrast to the $La_{1-x}Sr_xMnO_3$ and $La_{1-x}Ba_xMnO_3$ thin films [4–6]. Note that the line shape of the V $2p$ spectrum for the VO_2 thin film is identical to the previous work reported by Eguchi *et al.* [11]. In the case of W-doped VO_2 thin films, we evaluated V^* from the normalized I_S by the CI cluster model calculation, as mentioned later.

Figure 5 shows the valence-band HAXPES spectra of the $V_{1-x}W_xO_2$ thin films in the vicinity of E_F. The valence-band spectra for the $V_{1-x}W_xO_2$ thin films were normalized by the integrated intensity of the V $2p$ core-level spectra by a factor of $(1 - x)$, that is, the spectra were normalized by the

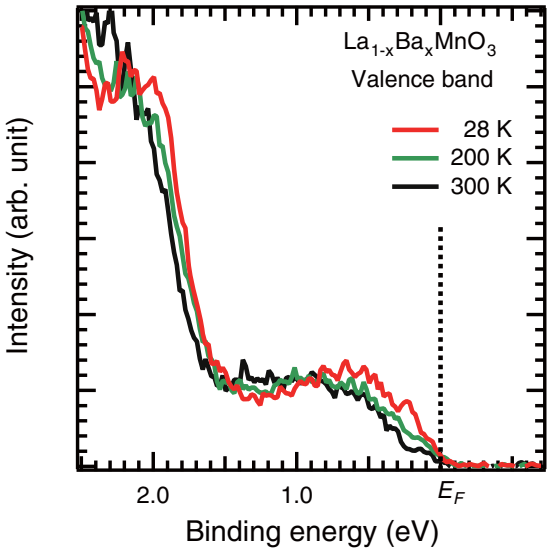

FIG. 3. (Color online) Valence band HAXPES spectra in the vicinity of E_F for the $La_{1-x}Ba_xMnO_3$ thin film with $x = 0.15$ taken at 28, 200, and 300 K.

V concentration. The $I(E_F)$ due to the V $3d$ states increased with the increasing of the W concentration (Fig. 5). The $I(E_F)$ does not show a simple relationship with the W concentration. Since the satellite structure, which arises from the metallic coherent screening process, was not easily separated from the main structure for the VO_2 thin film, we could not directly evaluate the normalized I_S from the V $2p$ core-level spectra for the $V_{1-x}W_xO_2$ thin films.

IV. CI CLUSTER MODEL CALCULATION

A. Mn $2p$ core level for the $La_{1-x}Ba_xMnO_3$ thin film

In order to qualitatively obtain the spectral weight of the satellite structure due to the coherent metallic screening process in the Mn $2p$ core-level spectra for the $La_{1-x}Ba_xMnO_3$ thin film, we have carried out the CI cluster model calculation, which takes the coherent metallic screening process into account according to the theoretical model by Taguchi *et al.* [9]:

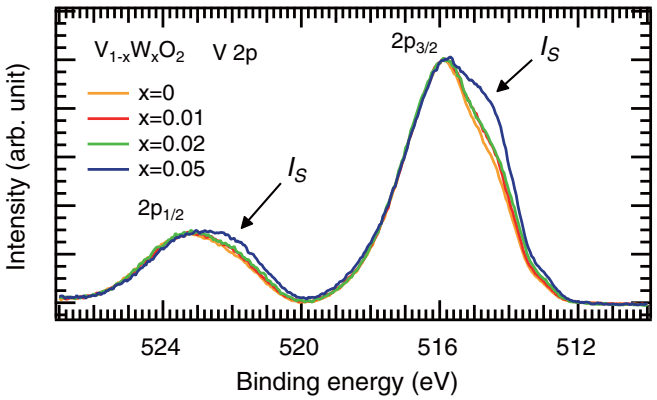

FIG. 4. (Color online) V $2p$ core-level HAXPES spectra for the $V_{1-x}W_xO_2$ thin films with $x = 0.00 - 0.05$ taken at 360 K. The spectra were normalized at $E_B = 515.94$ eV for comparison.

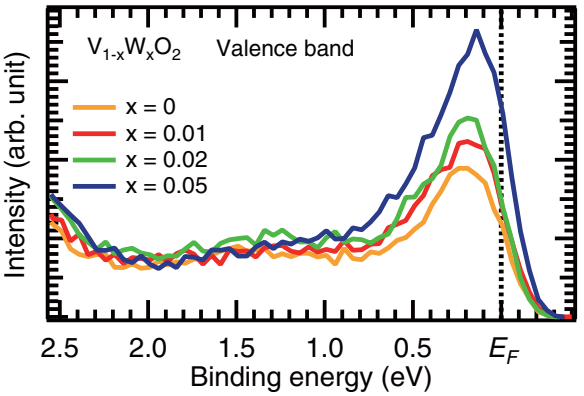

FIG. 5. (Color online) Valence band HAXPES spectra in the vicinity of E_F for the $V_{1-x}W_xO_2$ thin films [17]. The spectra were normalized by the V $2p$ core-level spectral intensity by a factor of $(1 - x)$.

$$H = H_{\rm I} + H_{\rm II} \tag{1}$$

$$H_{\rm I} = \sum_\sigma \varepsilon_{3d} d_\sigma^\dagger d_\sigma + \sum_\sigma \varepsilon_{2p} p_\sigma^\dagger p_\sigma + \sum_\sigma \varepsilon_p a_\sigma^\dagger a_\sigma + \sum_\sigma V_{pd}(d_\sigma^\dagger a_\sigma + a_\sigma^\dagger d_\sigma) + U_{dd} \sum_{\sigma\neq\sigma'} d_\sigma^\dagger d_\sigma d_{\sigma'}^\dagger d_{\sigma'} - U_{dc} \sum_{\sigma,\sigma'} d_\sigma^\dagger d_\sigma (1 - p_{\sigma'}^\dagger p_{\sigma'}), \tag{2}$$

$$H_{\rm II} = \sum_\sigma \varepsilon_c c_\sigma^\dagger c_\sigma + \sum_\sigma V^*(d_\sigma^\dagger c_\sigma + c_\sigma^\dagger d_\sigma). \tag{3}$$

The first term of Hamiltonian $H_{\rm I}$ in Eq. (1) represents the usual cluster model, and $H_{\rm II}$ represents the coherent metallic screening term [9]. The energies of the transition metal $3d$, $2p$, O $2p$ ligand, and coherent metallic states at around E_F are represented by ε_{3d}, ε_{2p}, ε_p, and ε_c, respectively. The index σ indicates the spin state. The hybridization strength between the transition metal $3d$ and ligand O $2p$ states, $3d$-$3d$, and $3d$-$2p$ Coulomb interactions are represented by V_{pd}, U_{dd}, and U_{dc}, respectively. The hybridization strength between the transition metal $3d$ and the coherent metallic states is represented by V^*.

The basis states of $|3d^4\rangle$, $|3d^5\underline{C}\rangle$, $|3d^3C\rangle$, and $|3d^5\underline{L}\rangle$ in the Mn ground state for $La_{1-x}Ba_xMnO_3$ are taken into account in the CI cluster model calculation, where $\underline{L}$ and $\underline{C}$ denote a hole in the ligand O $2p$ bands and coherent metallic states, respectively. The charge transfer energies are defined as $\Delta = E(3d^5\underline{L}) - E(3d^4)$ and $\Delta^* = E(3d^5\underline{C}) - E(3d^4)$. Each term is the center of gravity of multiplet states of the corresponding configuration. The $3d$-$3d$ and $3d$-$2p$ Coulomb interaction are denoted by $U_{dd} = E(3d^{n+1}) + E(3d^{n-1}) - 2E(3d^n)$ and $U_{dc} = [E(3d^{n+1}) - E(3d^n)] - [E(2p^5 3d^{n+1}) - E(2p^5 3d^n)]$, respectively. We neglected the multiplet states and band widths of the ligand O $2p$ bands and coherent metallic states in the calculation for simplicity. The schematic energy diagram of the initial and final states for the Mn $2p$ photoemission is shown in Fig. 6. The ground state $|g\rangle$ is given by the linear combination of the basis states of $|3d^4\rangle$, $|3d^5\underline{C}\rangle$, $|3d^3C\rangle$, and $|3d^5\underline{L}\rangle$ by

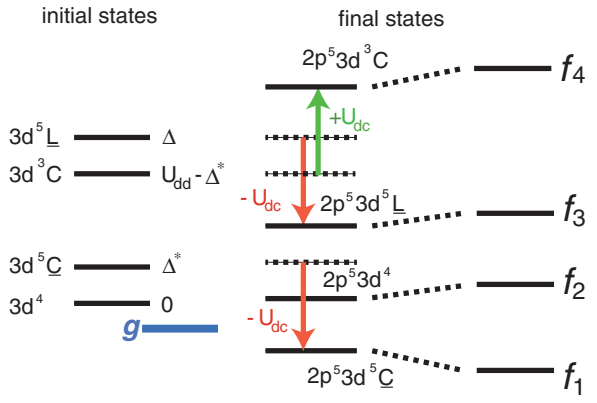

FIG. 6. (Color online) Schematic energy diagram of the initial and final states in the Mn $2p$ core-level photoemission for $La_{1-x}Ba_xMnO_3$. The ground state is denoted by g in the figure. The photoemission final states are denoted by f_n with $n = 1$–4. The electronic structure parameters of $\Delta = 4.5$ eV, $\Delta^* = 0.8$ eV, $U_{dd} = 5.1$ eV, $U_{dc} = 5.4$ eV, and $V_{pd} = 2.94$ eV were employed [6].

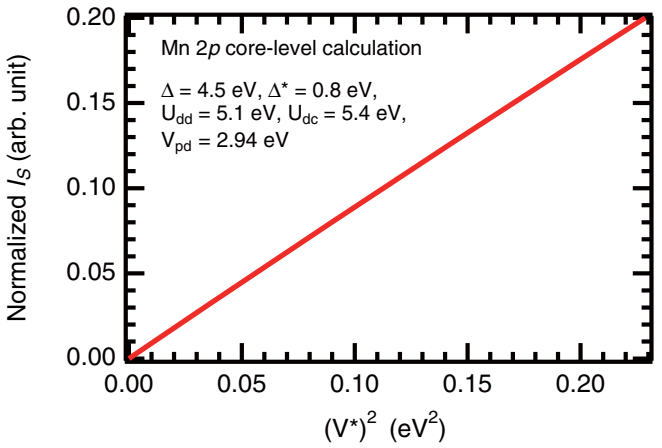

FIG. 7. (Color online) Calculated I_S as a function of $(V^*)^2$ for $La_{1-x}Ba_xMnO_3$, where I_S was normalized by $(I_{Mn2p} - I_S)$. The electronic structure parameters of $\Delta = 4.5$ eV, $\Delta^* = 0.8$ eV, $U_{dd} = 5.1$ eV, $U_{dc} = 5.4$ eV, and $V_{pd} = 2.94$ eV [6] were used as the fixed parameters for simplicity.

diagonalizing the secular equation, which is obtained by the Schrödinger equation using the Hamiltonian [Eqs. (1)–(3)]. The photoemission final states $|f_n\rangle$ with $n = 1$–4 for the Mn $2p$ core level are also obtained by the same sequence, where n is the index number of the final states (Fig. 6). The photoemission final states $|f_n\rangle$ are also given by the linear combination of the states of $|2p^53d^4\rangle$, $|2p^53d^5\underline{C}\rangle$, $|2p^53d^3C\rangle$, and $|2p^53d^5\underline{L}\rangle$ by diagonalizing the secular equation, which is obtained by the Schrödinger equation using the Hamiltonian [Eqs. (1)–(3)].

In the CI cluster model calculation, we used the electronic structure parameters of $\Delta = 4.5$ eV, $\Delta^* = 0.8$ eV, $U_{dd} = 5.1$ eV, $U_{dc} = 5.4$ eV, and $V_{pd} = 2.94$ eV [6] as the fixed parameters for simplicity. Since we used the experimental Mn $2p$ core-level spectra obtained in previous work [6], the electronic structure parameters determined by the CI cluster model calculation in the previous work were used in this paper. The photoemission intensities for the $|f_n\rangle$ final states with $n = 1$–4 were given by $I(f_n) = |\langle f_n|\boldsymbol{D}|g\rangle|^2$, where $\boldsymbol{D}$ is the dipole transition operator (i.e., the annihilation operator of one $2p$ core-level electron in this paper). The photoemission intensities for the $|f_n\rangle$ final states were calculated as a function of V^* in order to clarify the relationship between the normalized I_S and V^* in the case of $La_{1-x}Ba_xMnO_3$.

Figure 7 shows the calculated result of I_S normalized by $(I_{Mn2p} - I_S)$ as a function of $(V^*)^2$. Here I_{Mn2p} stands for the total photoemission intensity of the Mn $2p$ core level. I_S is due to the lowest energy state $|f_1\rangle$, which is caused by the metallic coherent screening effect, in the photoemission final states. We found that the calculation clearly exhibits the linear relationship between the normalized I_S and $(V^*)^2$.

B. V $2p$ core level for the $V_{1-x}W_xO_2$ thin films

In order to qualitatively obtain the spectral weight of the satellite structure due to the coherent metallic screening process in the V $2p$ core-level spectra for the $V_{1-x}W_xO_2$ thin film as well as that in the Mn $2p$ core-level spectra for the $La_{1-x}Ba_xMnO_3$ thin film, we have again carried out the CI cluster model calculation, which takes the coherent metallic screening process into account, according to Eqs. (1)–(3). According to Ref. [9], the basis states of $|3d^1\rangle$, $|3d^2\underline{C}\rangle$, $|3d^2\underline{L}\rangle$, $|3d^3\underline{C}^2\rangle$, $|3d^3\underline{L}C\rangle$, and $|3d^3\underline{L}^2\rangle$ in the V ground state are taken into account in the CI cluster model calculation, where $\underline{L}$ and $\underline{C}$ again denote a hole in the ligand O $2p$ bands and the coherent metallic states, respectively. The charge transfer energies are defined as $\Delta = E(3d^2\underline{L}) - E(3d^1)$ and $\Delta^* = E(3d^2\underline{C}) - E(3d^1)$. Each term is again the center of gravity of the multiplet states of the corresponding configuration. The hybridization strength between the V $3d$ and the ligand O $2p$ bands is represented by V_{pd}, while the hybridization strength between the V $3d$ states and the coherent metallic states is represented by V^*. The $3d$-$3d$ and $3d$-$2p$ Coulomb interactions are the same, as noted in Sec. IV A. Again, for simplicity, we neglected the multiplet states, the bandwidths of the ligand O $2p$ bands, and the coherent metallic states in the calculation. The schematic energy diagram of the initial and final states for the V $2p$ core-level photoemission is shown in Fig. 8. The ground state $|g\rangle$ is given by the linear combination of the basis states of $|3d^1\rangle$, $|3d^2\underline{C}\rangle$, $|3d^2\underline{L}\rangle$, $|3d^3\underline{C}^2\rangle$, $|3d^3\underline{L}C\rangle$, and $|3d^3\underline{L}^2\rangle$ by diagonalizing the secular equation, which is obtained by Schrödinger equation using the Hamiltonian shown in Eqs. (1)–(3). The photoemission final states $|f_n\rangle$ with $n = 1$–6 for the V $2p$ core level are also obtained by the same sequence, where n is the index number of the final states (Fig. 8). The photoemission final states $|f_n\rangle$ are also given by the linear combination of the states of $|2p^53d^1\rangle$, $|2p^53d^2\underline{C}\rangle$, $|2p^53d^2\underline{L}\rangle$, $|2p^53d^3\underline{C}^2\rangle$, $|2p^53d^3\underline{L}C\rangle$, and $|2p^53d^3\underline{L}^2\rangle$ by diagonalizing the secular equation, which is obtained by Schrödinger equation using the Hamiltonian shown in Eqs. (1)–(3).

In the CI cluster model calculation, we used the electronic structure parameters of $\Delta = 4.0$ eV, $\Delta^* = 0.2$ eV, $U_{dd} = 4.5$ eV, $U_{dc} = 6.5$ eV, and $V_{pd} = 2.4$ eV [11] as the fixed parameters for simplicity. Since our experimental V $2p$ core-level spectrum for VO_2 in the metallic phase was identical to the reported V $2p$ core-level spectrum for VO_2 by Eguchi *et al.* [11], the electronic structure parameters used in their CI cluster model

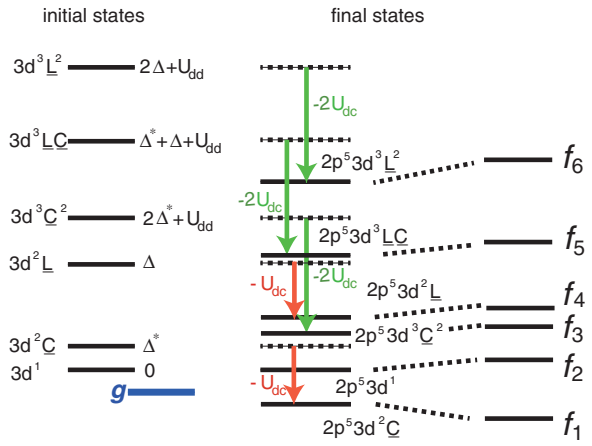

FIG. 8. (Color online) Schematic energy diagram of the initial and final states in the V $2p$ core-level photoemission for $V_{1-x}W_xO_2$. The ground state is denoted by g in the figure. The photoemission final states are denoted by f_n with $n = 1$–6. The electronic structure parameters of $\Delta = 4.0$ eV, $\Delta^* = 0.2$ eV, $U_{dd} = 4.5$ eV, $U_{dc} = 6.5$ eV, and $V_{pd} = 2.4$ eV were employed [11].

calculation were adapted in this paper. The photoemission intensities for the $|f_n\rangle$ final states with $n = 1$–6 were again given by $I(f_n) = |\langle f_n|\boldsymbol{D}|g\rangle|^2$. The photoemission intensities for the$|f_n\rangle$ final states were calculated as a function of V^* in order to clarify the relationship between the normalized I_S and V^* in the case of $V_{1-x}W_xO_2$. We note that the spectral weight for the highest final state $|f_6\rangle$ has been extracted from the V $2p$ core-level photoemission intensity from the comparison between the calculated and experimental results because the highest final state energy is significantly far from the others and does not contribute to the V $2p$ core-level spectra in the E_B range between 511 and 527 eV in the case of $V_{1-x}W_xO_2$.

Figures 9(a) and 9(b) show the calculated result of I_S normalized by $(I_{V2p} - I_S)$ as a function of (V^*) and $(V^*)^2$, respectively. Here, I_{V2p} stands for the total photoemission intensity of the V $2p$ core level excluding the highest final state. I_S is due to the lowest energy state $|f_1\rangle$, which is caused by the metallic coherent screening effect, in the photoemission final states. We found that the normalized I_S is neither proportional to (V^*) nor $(V^*)^2$, in contrast to the calculated result of the normalized I_S for the Mn $2p$ core-level photoemission in $La_{1-x}Ba_xMnO_3$, as seen in Fig. 7.

V. DISCUSSION

Let us consider the behavior of the normalized I_S in the Mn $2p$ and V $2p$ core-level spectra for $La_{1-x}Ba_xMnO_3$ and $V_{1-x}W_xO_2$, respectively. As seen in Figs. 2(b) and 7, the normalized I_S in the Mn $2p$ core-level spectra for $La_{1-x}Ba_xMnO_3$ is proportional to $(V^*)^2$. In contrast, as seen in Fig. 9, the normalized I_S in the V $2p$ core-level spectra for $V_{1-x}W_xO_2$ is neither proportional to V^* nor $(V^*)^2$. The different behavior of the normalized I_S in the Mn $2p$ and V $2p$ core-level spectra can be understood by the energy diagram of the initial and final states in the core-level photoemission process, as mentioned later.

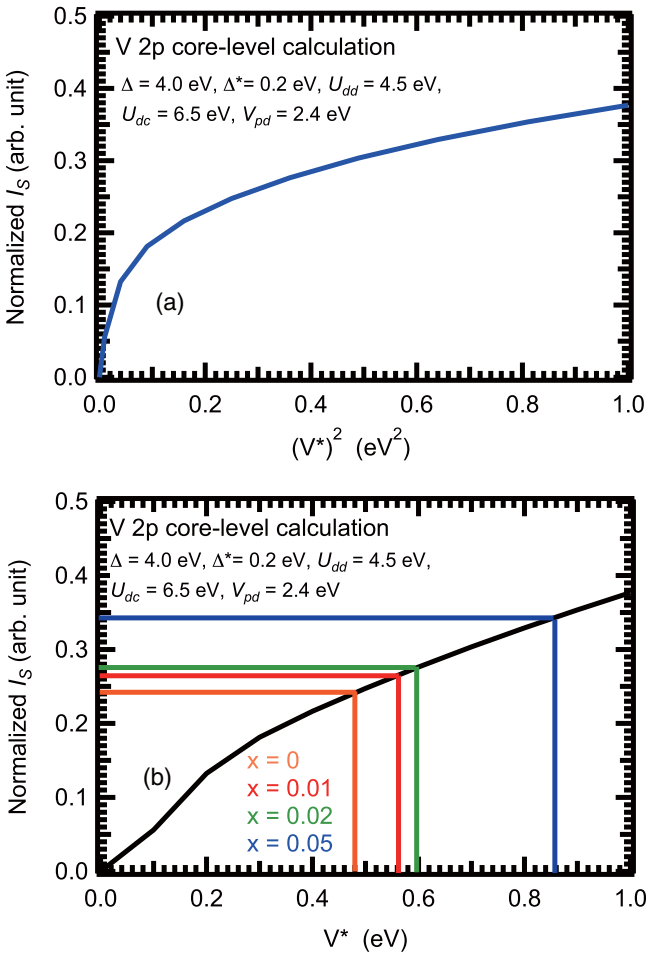

FIG. 9. (Color online) (a) Calculated I_S as a function of $(V^*)^2$ and (b) as a function of V^* for $V_{1-x}W_xO_2$, where I_S was normalized by $(I_{V2p} - I_S)$. The electronic structure parameters of $\Delta = 4.0$ eV, $\Delta^* = 0.2$ eV, $U_{dd} = 4.5$ eV, $U_{dc} = 6.5$ eV, and $V_{pd} = 2.4$ eV [11] were used as the fixed parameters for simplicity.

In the case of $La_{1-x}Ba_xMnO_3$ (shown in Fig. 6), the energy separation of the lowest two $|3d^4\rangle$ and $|3d^5\underline{C}\rangle$ states in the initial states is defined by Δ^*, as mentioned in Sec. IV, and Δ^* of 0.8 eV was employed in the series of the CI cluster model calculation. The other two states in the initial states are separated above 4.3 eV from the lowest $|3d^4\rangle$ state. Therefore, the ground state is dominated by the $|3d^4\rangle$ state. A small amount of the $|3d^5\underline{C}\rangle$ state is mixed in the ground state. In the Mn $2p$ core-level photoemission final states, the lowest term is dominated by the $|2p^53d^5\underline{C}\rangle$ state due to the Coulomb interaction of U_{dc} between the $2p$ core hole and $3d$ electrons, as seen in Fig. 5. And the second-lowest term dominated by the $|2p^53d^4\rangle$ state is separated by $|\Delta - U_{dc}|$ of 4.6 eV. The other states are further separated from the lowest term in the final states, as seen in Fig. 6. Therefore, we see that the main and satellite structures in the Mn $2p$ core-level spectra are dominated by the $|2p^53d^4\rangle$ and $|2p^53d^5\underline{C}\rangle$ states, respectively. Since a small amount of the $|3d^5\underline{C}\rangle$ state in the ground state and the corresponding final state of $|2p^53d^5\underline{C}\rangle$ state became the lowest final states, which was sufficiently separated from the other final states, we found that the normalized I_S is

proportional to $(V^*)^2$ from the series of the CI cluster model calculations, as seen in Fig. 7.

One sees in Figs. 2(b) and 7 that the inclination angle of the normalized I_S as a function of $(V^*)^2$ is different between the experiment and CI cluster model calculation. Since the Mn^{4+} derived state appears in the higher E_B side of the Mn $2p_{3/2}$ main peak and is not included in the CI cluster model calculation [4], the normalized I_S for the calculation shown in Fig. 7 is about two times larger than that obtained from the experiments shown in Fig. 2(b). But this deviation can be compensated by multiplying a factor, which value is estimated from the comparison between the experimental and theoretical normalized I_S values.

In contrast to the behavior of the normalized I_S in the Mn $2p$ core-level spectra for $La_{1-x}Ba_xMnO_3$, the normalized I_S in the V $2p$ core-level spectra for $V_{1-x}W_xO_2$ does not show a linear relationship to $(V^*)^2$. This is due to the small Δ^* between the lowest two states of $|3d^1\rangle$ and $|3d^2\underline{C}\rangle$ in the initial states (Fig. 8). The main component of the ground state is $|3d^1\rangle$, while a relative large amount of $|3d^2\underline{C}\rangle$ is also mixing in the ground state due to the small value of Δ^*, in contrast to the case of $La_{1-x}Ba_xMnO_3$. The other states in the initial states are separated above 4 eV from the lowest state (Fig. 8). In the V $2p$ photoemission final states, the lowest state is mainly due to $|2p^53d^2\underline{C}\rangle$ because the $2p$ core hole state is well screened by an additional $3d$ electron in comparison with $|2p^53d^1\rangle$ (Fig. 8). The strong mixing of $|3d^1\rangle$ and $|3d^2\underline{C}\rangle$ in the ground state, however, strongly affects the compositions of $|2p^53d^1\rangle$ and $|2p^53d^2\underline{C}\rangle$ states through the hybridization due to the metallic coherent screening effect in the lowest photoemission final state. Therefore, the normalized I_S is mainly due to $|2p^53d^2\underline{C}\rangle$, but the mixing of $|2p^53d^1\rangle$ to the normalized I_S cannot be negligible. In addition the small energy separation among three $|2p^53d^1\rangle$, $|2p^53d^3\underline{C}^2\rangle$, and $|2p^53d^2\underline{L}\rangle$ components in the photoemission final states, which mainly compose the main peak structure of the V $2p$ core-level spectra for $V_{1-x}W_xO_2$, is also affected through the hybridization. Therefore the normalized I_S in the V $2p$ core-level spectra for $V_{1-x}W_xO_2$ shows a nonlinear relationship between the normalized I_S and $(V^*)^2$.

In Fig. 9(b), we estimated the normalized I_S for $V_{1-x}W_xO_2$ with $x = 0$ from the CI cluster model calculation, and the experimental normalized I_S for $V_{1-x}W_xO_2$ with $x \neq 0$ was then obtained by referring the V $2p$ core-level spectrum for $V_{1-x}W_xO_2$ with $x = 0$. Since the ratio of the normalized I_S to the total V $2p$ core-level photoemission intensity for $V_{1-x}W_xO_2$ with $x = 0$ can be obtained from the calculation, the normalized I_S for $V_{1-x}W_xO_2$ with $x \neq 0$ is obtained by subtracting the V $2p$ core-level spectrum for $x \neq 0$ from that for $x = 0$.

Figure 10 shows the $I(E_F)$ as a function of $(V^*)^2$ for the $La_{1-x}Ba_xMnO_3$ thin film. As seen in Fig. 10, the $I(E_F)$ was proportional to $(V^*)^2$, which was expected from the framework of AIM. In the case of the $V_{1-x}W_xO_2$ thin films, we found that $I(E_F)$ is proportional to $(V^*)^2$ (Fig. 11), which was also expected from the framework of AIM. These results support that the DOS at E_F is proportional to $(V^*)^2$. Thus, when we have one reference data of the electronic structure parameters, which reproduce the experimental spectrum well, we can estimate V^* from the comparison of the experimental spectra and the CI cluster model calculation.

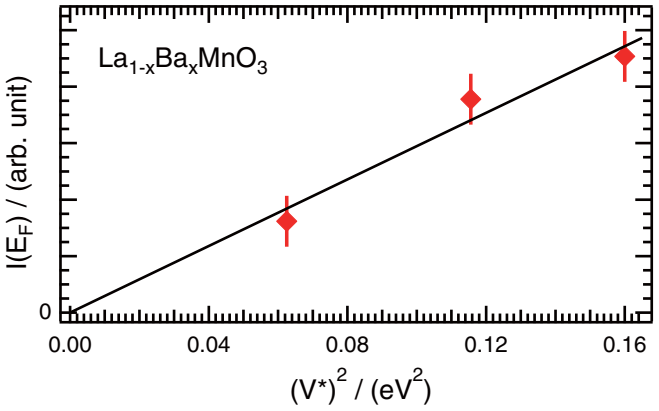

FIG. 10. (Color online) Relationship between the experimental $I(E_F)$ and evaluated $(V^*)^2$ for $La_{1-x}Ba_xMnO_3$. The solid line corresponds to the least-square-fitting result.

As mentioned above, the behavior of the normalized I_S for $La_{1-x}Ba_xMnO_3$ and $V_{1-x}W_xO_2$ as a function of V^* was explained by the different trends in the electronic structure parameters in the CI cluster model calculations. The linear relationship between the normalized I_S and $(V^*)^2$ in the Mn $2p$ core-level spectra for $La_{1-x}Ba_xMnO_3$ was well explained by the CI cluster model calculation. The nonlinear relationship between the normalized I_S and $(V^*)^2$ in the V $2p$ core-level spectra for $V_{1-x}W_xO_2$ was also well explained by the CI cluster model calculation. These results suggest that the electronic structure parameters in these systems play important roles in the evolution of I_S as a function of V^* in the strongly correlated oxides, which show the coherent metallic screening process in the core-level photoemission.

As seen in Figs. 1 and 3, the small intensity changes at E_F for the $La_{1-x}Ba_xMnO_3$ thin film strongly affect the satellite intensity in the Mn $2p$ core-level spectra. This tendency was also seen in the case of the $V_{1-x}W_xO_2$ thin films. These results indicate that I_S due to the metallic coherent screening process is very sensitive to the DOS at E_F, and the CI cluster model approach according to Taguchi *et al.* [9] is very useful for analyzing the electronic structures of the strongly correlated

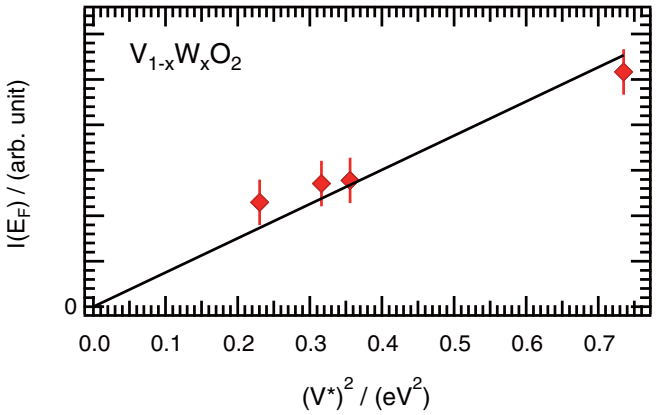

FIG. 11. (Color online) Relationship between the experimental $I(E_F)$ and evaluated $(V^*)^2$ for $V_{1-x}W_xO_2$. The solid line corresponds to the least-square-fitting result.

oxides, which show the coherent metallic screening process in the core-level photoemission. The $I(E_F)$ (i.e., DOS at E_F) are attributed to the Mn and V 3d states for $La_{1-x}Ba_xMnO_3$, and $V_{1-x}W_xO_2$, respectively. Thus, these results strongly support that the CI cluster model appropriately treats the 3d electronic states having both the localized and delocalized character in the strongly correlated system by introducing the coherent metallic states. This CI cluster model approach is thus very useful for evaluating and understanding the electronic structures of the strongly correlated systems instead of using the multisite cluster model [20,21].

VI. SUMMARY

We have performed the HAXPES measurements and the CI cluster model calculation for the strongly correlated $La_{1-x}Ba_xMnO_3$ and $V_{1-x}W_xO_2$ thin films in order to investigate the variation of I_S due to the coherent metallic screening effect in the photoemission final states. The Mn 2p core-level HAXPES spectra for $La_{1-x}Ba_xMnO_3$ showed that the clear temperature dependence on I_S was due to the coherent metallic screening process. The V 2p core-level HAXPES spectra for $V_{1-x}W_xO_2$ also showed that the clear W-doping dependence on I_S was due to the coherent metallic screening process. The variation of I_S found in $La_{1-x}Ba_xMnO_3$ showed the linear relationship between normalized I_S and $(V^*)^2$. The CI cluster model, including the coherent metallic screening process, reproduced well the linear relationship of normalized I_S and $(V^*)^2$. In contrast, normalized I_S for $V_{1-x}W_xO_2$ was neither proportional to V^* nor $(V^*)^2$. We found that $I(E_F)$ for $La_{1-x}Ba_xMnO_3$ and $V_{1-x}W_xO_2$ is proportional to $(V^*)^2$, which can be deduced from AIM. Our results showed that the simplified CI cluster model calculation is useful for evaluating the electronic structure parameters, in particular V^*, in the systematic electronic structure study when one has a reference electronic structure parameters set, which reproduces an experimental core-level spectrum, as a guide for the calculations. These results strongly support that the CI cluster model appropriately treats the 3d electronic states having both the localized and delocalized character in the strongly correlated system by introducing the coherent metallic states and is very useful for evaluating and understanding the electronic structures of the strongly correlated systems.

ACKNOWLEDGMENTS

The authors would like to thank the staff of BL29XU and BL15XU of SPring-8 for their help during the HAXPES measurements. We also appreciate the staff of HiSOR, Hiroshima University and JAEA/SPring-8 for the development of HAXPES at BL15XU of SPring-8. The HAXPES experiments were performed with the approval of JASRI/SPring-8 and NIMS Beamline Station at SPring-8 (Proposals No. 2006A1606 and No. 2009B4904). This work was partially supported by the Ministry of Education, Culture, Sports, Science and Technology (MEXT), Japan.

[1] N. A. van Veenendaal and G. A. Sawatzky, Phys. Rev. B **49**, 1407 (1994).
[2] K. Okada, Surf. Rev. Lett. **9**, 1023 (2002).
[3] M. Taguchi, A. Chainani, K. Horiba, Y. Takata, M. Yabashi, K. Tamasaku, Y. Nishino, D. Miwa, T. Ishikawa, T. Takeuchi, K. Yamamoto, M. Matsunami, S. Shin, T. Yokoya, E. Ikenaga, K. Kobayashi, T. Mochiku, K. Hirata, J. Hori, K. Ishii, F. Nakamura, and T. Suzuki, Phys. Rev. Lett. **95**, 177002 (2005).
[4] K. Horiba, M. Taguchi, A. Chainani, Y. Takata, E. Ikenaga, D. Miwa, Y. Nishino, K. Tamasaku, M. Awaji, A. Takeuchi, M. Yabashi, H. Namatame, M. Taniguchi, H. Kumigashira, M. Oshima, M. Lippmaa, M. Kawasaki, H. Koinuma, K. Kobayashi, T. Ishikawa, and S. Shin, Phys. Rev. Lett. **93**, 236401 (2004).
[5] K. Horiba, A. Maniwa, A. Chikamatsu, K. Yoshimatsu, H. Kumigashira, H. Wadati, A. Fujimori, S. Ueda, H. Yoshikawa, E. Ikenaga, J. J. Kim, K. Kobayashi, and M. Oshima, Phys. Rev. B **80**, 132406 (2009).
[6] H. Tanaka, Y. Takata, K. Horiba, M. Taguchi, A. Chainani, S. Shin, D. Miwa, K. Tamasaku, Y. Nishino, T. Ishikawa, E. Ikenaga, M. Awaji, A. Takeuchi, T. Kawai, and K. Kobayashi, Phys. Rev. B **73**, 094403 (2006).
[7] S. Ueda, H. Tanaka, E. Ikenaga, J. J. Kim, T. Ishikawa, T. Kawai, and K. Kobayashi, Phys. Rev. B **80**, 092402 (2009).
[8] N. Kamakura, M. Taguchi, A. Chainani, Y. Takata, K. Horiba, K. Yamamoto, K. Tamasaku, Y. Nishino, D. Miwa, E. Ikenaga, M. Awaji, A. Takeuchi, H. Ohashi, Y. Senba, H. Namatame, M. Taniguchi, T. Ishikawa, K. Kobayashi, and S. Shin, Europhys. Lett. **68**, 557 (2004).
[9] M. Taguchi, A. Chainani, N. Kamakura, K. Horiba, Y. Takata, M. Yabashi, K. Tamasaku, Y. Nishino, D. Miwa, T. Ishikawa, S. Shin, E. Ikenaga, T. Yokoya, K. Kobayashi, T. Mochiku, K. Hirata, and K. Motoya, Phys. Rev. B **71**, 155102 (2005).
[10] S. Suga, A. Sekiyama, S. Imada, T. Miyamachi, H. Fujiwara, A. Yamasaki, K. Yoshimura, K. Okada, M. Yabashi, K. Tamasaku, A. Higashiya, and T. Ishikawa, New J. Phys. **11**, 103015 (2009).
[11] R. Eguchi, M. Taguchi, M. Matsunami, K. Horiba, K. Yamamoto, Y. Ishida, A. Chainani, Y. Takata, M. Yabashi, D. Miwa, Y. Nishino, K. Tamasaku, T. Ishikawa, Y. Senba, H. Ohashi, Y. Muraoka, Z. Hiroi, and S. Shin, Phys. Rev. B **78**, 075115 (2008).
[12] H. Takami, T. Kanki, S. Ueda, K. Kobayashi, and H. Tanaka, Appl. Phys. Express **3**, 063201 (2010).
[13] K. Kobayashi, M. Yabashi, Y. Takata, T. Tokushima, S. Shin, K. Tamasaku, D. Miwa, T. Ishikawa, H. Nohira, T. Hattori, Y. Sugita, O. Nakatsuka, S. Sakai, and S. Zaima, Appl. Phys. Lett. **83**, 1005 (2003).

[14] Y. Takata, M. Yabashi, K. Tamasaku, Y. Nishino, D. Miwa, T. Ishikawa, E. Ikenaga, K. Horiba, S. Shin, M. Arita, K. Shimada, H. Namatame, M. Taniguchi, H. Nohira, T. Hattori, S. Sodergren, B. Wannberg, and K. Kobayashi, Nucl. Instrum. Methods Phys. Res., Sect. A **547**, 50 (2005).

[15] S. Tanuma, C. J. Powell, D. R. Penn, Surf. Interface Anal. **21**, 165 (1994).

[16] O. Gunnarsson and K. Schonehammer, in *Handbook on the Physics and Chemistry of Rare Earths*, edited by K. A. Gschneider, Jr., L. Eyring, and S. Hufner, Vol. 10 (Elsevier Science Publishers B.V., New York, 1987).

[17] H. Takami, T. Kanki, S. Ueda, K. Kobayashi, and H. Tanaka, Phys. Rev. B **85**, 205111 (2012).

[18] H. Takami, K. Kawatani, T. Kanki, and H. Tanaka, Jpn. J. Appl. Phys. **50**, 055804 (2011).

[19] S. Ueda, Y. Katsuya, M. Tanaka, H. Yoshikawa, Y. Yamashita, S. Ishimaru, Y. Matsushita, and K. Kobayashia, AIP Conf. Proc. **1234**, 403 (2010).

[20] M. A. van Veenendaal, H. Eskes, and G. A. Sawatzky, Phys. Rev. B **47**, 11462 (1993).

[21] K. Okada and A. Kotani, J. Electron Spectrosc. Relat. Phenom. **86**, 119 (1997).